



ELSEVIER

journal homepage: www.intl.elsevierhealth.com/journals/cmpb

Segmentation and detection of breast cancer in mammograms combining wavelet analysis and genetic algorithm



Danilo Cesar Pereira^{a,1}, Rodrigo Pereira Ramos^{b,*},
Marcelo Zanchetta do Nascimento^{c,1}

^a Centro de Matemática, Computação e Cognição, Universidade Federal do ABC, Rua Santa Adélia, 166, 09210170 Santo André, SP, Brazil

^b Colegiado de Engenharia Elétrica, Universidade Federal do Vale do São Francisco, Avenida Antônio Carlos Magalhães, 510, 48902300 Juazeiro, BA, Brazil

^c Faculty of Computation (FACOM), Federal University of Uberlândia (UFU), Av. João Naves de Ávila, 2121, 38400902 Uberlândia, MG, Brazil

ARTICLE INFO

Article history:

Received 6 February 2013

Received in revised form

9 January 2014

Accepted 14 January 2014

Keywords:

Wavelet transform

Genetic algorithm

Mammographic images

Image segmentation

Computer-aided systems

ABSTRACT

In Brazil, the National Cancer Institute (INCA) reports more than 50,000 new cases of the disease, with risk of 51 cases per 100,000 women. Radiographic images obtained from mammography equipments are one of the most frequently used techniques for helping in early diagnosis. Due to factors related to cost and professional experience, in the last two decades computer systems to support detection (Computer-Aided Detection – CADe) and diagnosis (Computer-Aided Diagnosis – CADx) have been developed in order to assist experts in detection of abnormalities in their initial stages. Despite the large number of researches on CADe and CADx systems, there is still a need for improved computerized methods. Nowadays, there is a growing concern with the sensitivity and reliability of abnormalities diagnosis in both views of breast mammographic images, namely crano-caudal (CC) and medio-lateral oblique (MLO). This paper presents a set of computational tools to aid segmentation and detection of mammograms that contained mass or masses in CC and MLO views. An artifact removal algorithm is first implemented followed by an image denoising and gray-level enhancement method based on wavelet transform and Wiener filter. Finally, a method for detection and segmentation of masses using multiple thresholding, wavelet transform and genetic algorithm is employed in mammograms which were randomly selected from the Digital Database for Screening Mammography (DDSM). The developed computer method was quantitatively evaluated using the area overlap metric (AOM). The mean \pm standard deviation value of AOM for the proposed method was $79.2 \pm 8\%$. The experiments demonstrate that the proposed method has a strong potential to be used as the basis for mammogram mass segmentation in CC and MLO views. Another important aspect is that the method overcomes the limitation of analyzing only CC and MLO views.

© 2014 Elsevier Ireland Ltd. All rights reserved.

* Corresponding author. Tel.: +55 74 2102 7630; fax: +55 74 2102 7630.

E-mail addresses: danilo.pereira@ufabc.edu.br (D.C. Pereira), rodrigo.ramos@univasf.edu.br, [\(R.P. Ramos\)](mailto:godoga@gmail.com), marcelo.zanchetta@gmail.com, nascimento@facom.ufu.br (M.Z. do Nascimento).

¹ Tel.: +55 34 3239 4571; fax: +55 34 3239 4571.

0169-2607/\$ – see front matter © 2014 Elsevier Ireland Ltd. All rights reserved.

<http://dx.doi.org/10.1016/j.cmpb.2014.01.014>

1. Introduction

Over the past few years, the cancer has been one of the most responsible for the high number of deaths, and could become one of the main responsible for most deaths in the next decades. According to the World Health Organization, the number of deaths due to cancer, which was just 13% in 2008, is currently having a significant increase and one estimates that this number could reach approximately 12 million until 2030 [1].

Breast cancer is the second-most common and leading cause of cancer death among women. In Brazil, the National Cancer Institute (INCA) reports more than 50,000 new cases of the disease, with risk of 51 cases per 100,000 women [2]. Since it still has unknown causes, a large technology investment and a large number of human resources have to be available for early detection in order to reduce the mortality rate of the patients.

The screen-film mammography is an important tool used by radiologists to detect cancer at an early stage. In this examination, four images are obtained, two corresponding to the right breast and two to the left breast of the projections crano-caudal (CC) and medio-lateral oblique (MLO). The use of CC and MLO images improves visualization of breast tissue and increases the chances of detecting the presence of non-palpable breast cancer. During the examination, the radiologist combines information from these two views to increase the chances of determining a priori regions with abnormalities defined as true positive (TP) and reduce the number of regions without abnormalities, i.e., reduce false positive (FP) regions [3]. However, screen-film mammography is a repetitive task, making radiologists prone to oversight errors. As a result, radiologists fail to detect from 10% up to 30% of malignant lesion on mammograms [4].

Recently, Computer-Aided Detection (CADe) and Computer-Aided Diagnosis (CADx) have been applied to mammographic images to assist radiologists on lesions analysis such as microcalcification, mass and architectural distortions [5]. CADe schemes automatically detect and segment suspicious lesions in mammograms, i.e., perform a localization task. CADx systems extend the computer analysis to characterize suspicious regions or estimate the probability of malignancy of a lesion, and are focused on the classification task. For a survey of the state of the art of CADx systems, the reader is referred to a recent review article [6]. The present work is focused on an automatic segmentation system of suspicious lesions for mammographic images.

In spite of the relevant research contributions for the area, CADe systems exhibit different performances on detecting and/or segmenting mass lesions or microcalcification clusters. Specifically for microcalcifications, recent papers show some progress for automatic detection methods, reaching sensitivity rates of about 98%. However, mass detection is a more complex task, because the mass is frequently indistinguishable from adjacent tissues. Mass detection poses a difficult challenge because masses are often: (a) very pronounced in size, shape and density; (b) poor in image contrast; (c) highly connected to the surrounding parenchymal tissue density, particularly for speculated lesions and (d) surrounded by no

uniform tissue background with similar characteristics [7]. That makes progress be considerably slow for reliable detection of masses.

To improve diagnostic accuracies, the strategy of double reading has been used to increase the sensitivity level. However, the double reading performed by two radiologists increases operating costs and it is not always available. Comparing mammographic images from the same patient is a common practice for diagnosis purposes. Usually, images from both views (CC and MLO) of the same breast are compared. Some researches show that this approach can improve detection and diagnosis performances in contrast to employing a single mammographic view [8–11]. This methodology reduces patient recalls for a second inspection. Frequently, CADe commercial systems operate independently on each mammographic view. Nevertheless, there are situations when the system detects abnormalities in only one of the views. Radiologists believe that there is an inconsistency when a given lesion is not found, still being perceptible on both views, leading to a system reliability reduction and indicating that those results can be ignored. Several authors have been conducting researches to build CADe systems that can analyze two views on breast cancer detection [10,11].

The present work shows a set of computer-aided tools developed for segmentation of masses using two views, namely CC and MLO mammographic projections. To eliminate built-in patient informations, an algorithm is firstly applied to remove artifacts present at the mammograms background. To reduce the degradation/noise occurring in the process of image acquisition, a pre-processing technique based on Wiener filtering in the wavelet domain was applied to each image. After that, a computational process combining genetic algorithm (GA) and wavelet transform was employed to determine an appropriate number of threshold levels as well as the values of these levels required to mass segmentation. The GA and wavelet combination was used to decrease computational times for threshold selection. The threshold levels were then used in a multimodal thresholding procedure for detection and segmentation of masses obtained from CC and MLO views. The proposed computational tools were evaluated on a set of selected cases from the public Digital Database for Screening Mammography (DDSM) [12].

This article is organized as follows: in Section 2, it is described the algorithm employed on artifact elimination, breast image enhancement and multimodal segmentation of images obtained from both views. Section 3 presents experimental results obtained with the developed algorithm. Section 4 shows result discussions and conclusions of the work.

2. Materials and methods

This section describes the procedures employed for mammogram masses segmentation considering both CC and MLO views. Fig. 1 presents the block diagram of the applied algorithms.

2.1. Artifacts elimination

The performance of segmentation algorithms can be influenced by several factors such as artifacts and personal patient

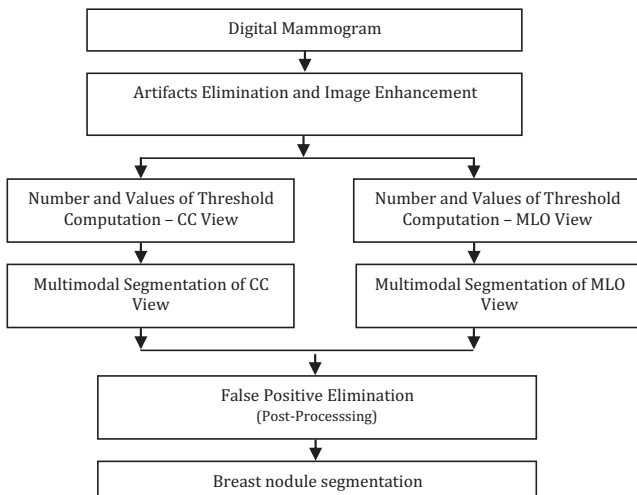


Fig. 1 – Block diagram of the computational algorithms developed for segmentation of masses using mammographic images acquired from both CC and MLO views.

informations, which are marked on the image by lead blocks. To improve the performance of segmentation techniques used later in this article, it was applied an algorithm (Fig. 2(a)) for removing artifacts on each image. This procedure employs a top-hat morphological operation, with a structuring element with a 60 pixels radius, whose mathematical representation is given below:

$$OP_{top} = \max[0, f(x, y) - (f \circ B)(x, y)]. \quad (1)$$

where:

$$(f \circ B)(x, y) = [(f \ominus B)(x, y) \otimes B](x, y) \quad (2)$$

$$(f \ominus B)(x, y) = \max[(f(x - t_1, y - t_2), (t_1, t_2) \in B)] \quad (3)$$

$$(f \otimes B)(x, y) = \max[(f(x + t_1, y + t_2), (t_1, t_2) \in B)] \quad (4)$$

with $f(x, y)$ being the mammographic image and B the structuring element, both defined over the set Z^2 , and (t_1, t_2) is a pair of pixels of the structuring element B .

In a next step, a subtraction was performed between the resulting and the original images (Fig. 2(c)), and then Otsu's method for automatic thresholding [13] was applied to the image resulted from subtraction (Fig. 2(d)) as specified by Eqs. (5) and (6):

$$\sigma_\omega^2(t) = \omega_1(t)\sigma_1^2(t) + \omega_2(t)\sigma_2^2(t) \quad (5)$$

$$\sigma_b^2(t) = \sigma^2 - \sigma_\omega^2(t) = \omega_1(t)\omega_2(t)[\mu_1(t) + \mu_2(t)]^2 \quad (6)$$

where $\omega_1(t)$ and $\omega_2(t)$ represents the separation probabilities for the first and second regions (or classes), respectively, t is the threshold value, σ_1^2 and σ_2^2 are the variances of each class, and μ_1 and μ_2 are the classes mean values.

Following, a multiplication was performed between the Otsu's method output image and the original one, yielding an image with no background artifacts (see Fig. 2(e)).

2.2. Enhancement based on wavelet multiresolution processing

The enhancement step aims to provide information improvement of the breast internal structures and confer better results on the detection and segmentation processes of mammographic image regions. Traditional algorithms, such as histogram equalization, gradient enhancement, and spatial filtering present difficulties in providing relevant results for medical image processing. Several enhancement algorithms have been proposed in literature [14,15] using different approaches for visual improvement of mammographic images. Recent studies have shown that the use of wavelet theory provides better results in the step of medical images enhancement. Therefore, as a way to acquire good image enhancement results, it was developed an algorithm based on wavelet multiresolution theory and Wiener filtering [16,17].

Image analysis in multiple scales allows image resolution to be changed so as to process as little data as possible by selecting relevant details for a given visual task [18]. The basic idea of multiresolution analysis is to represent an image on several sub-images, from coarse to fine resolution, and analyze them in the frequency domain. Broadly speaking, multiresolution allows for the zooming in or out on an image, when this is necessary.

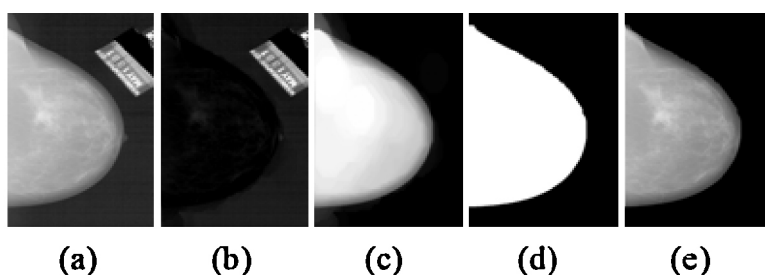


Fig. 2 – Output images from artifact elimination algorithm: (a) mammographic image of CC view, obtained from case 1134; (b) image modified by top-hat morphological operation; (c) image resulting from subtraction operation; (d) image followed from Otsu's thresholding; (e) image without artifacts obtained from the multiplication step.

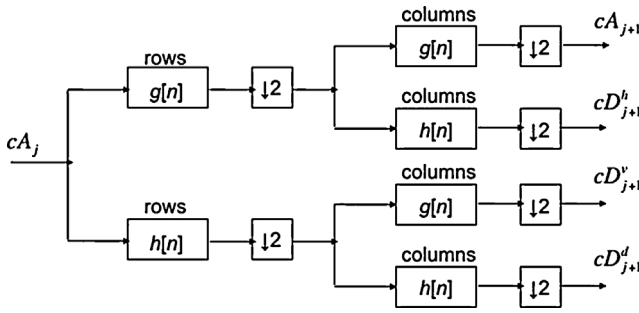


Fig. 3 – One stage of a 2D-DWT filter bank.

A wavelet is a function $\psi(x) \in L^2(\mathbb{R})$ (the set of square integrable functions), with a zero average:

$$\int_{-\infty}^{\infty} \psi(x) dx = 0 \quad (7)$$

which is normalized to have unit energy and centered in the neighborhood of $x=0$. Given a function $f(x) \in \mathbb{R}$, its wavelet transform $Wf(s, u) \in \mathbb{R}$ is obtained from the inner product of $f(x)$ and a wavelet family, i.e.:

$$Wf(s, u) = \int_{-\infty}^{\infty} f(x) \psi_{s,u}(x) dx \quad (8)$$

where

$$\psi_{s,u}(x) = \frac{1}{\sqrt{s}} \psi\left(\frac{x-u}{s}\right) \quad (9)$$

is the wavelet family obtained by scaling $\psi(x)$ by s (the scale parameter) and translating it by u (the translation parameter). The scale s is referred to as the transform resolution level.

For discrete signals, the discrete wavelet transform (DWT) is obtained by the discretization of time as well as the translation and scale parameters. The most common discretization is the dyadic wavelet decomposition, which is achieved when $s=2^j$ and $u=k 2^j$, for integers j and k . Due to its relation to the scale parameter, j is referred to as the resolution level of the dyadic wavelet transform. Mallat [19] has proved that the dyadic DWT of a signal is equivalent to its decomposition through high-pass ($g[n]$) and low-pass ($h[n]$) filter banks, composed of as many banks as is the desired resolution. When dealing with images, which are 2-dimensional signals, the DWT can be computed with separable wavelet functions, what means that a 2-dimensional filter can be decomposed as the product of two one-dimensional filters. In this case, a 1D-DWT is computed first in the image rows, and another 1D-DWT is applied to the columns of the two images generated. The 2D-DWT is illustrated in Fig. 3, in which an original image at the j -th level (cA_j coefficients) is wavelet transformed, yielding 4 sub-band images at the $(j+1)$ -th level. There are 3 detail images, cD_{j+1}^h , cD_{j+1}^v , and cD_{j+1}^d , that represents horizontal, vertical and diagonal directions, respectively, and one approximation image cA_{j+1} , which is the original image at a coarse resolution.

Many wavelet families have been developed and there are several possibilities for choosing a given family to compute

the image wavelet transform. Each wavelet has distinct characteristics that allow for a better context adaptation. Haar, Daubechies and Coiflets were analyzed in the image contrast enhancement step, and each image was decomposed on three resolution levels by the 2D-DWT, for each wavelet family. The choice of three resolution levels was based on minimizing computational complexity without affecting the system performance. Some previous results have used four resolution levels [20] for mass boundaries revealing. However, at the initial time the present work started, some computational tests have showed similar results when using either three or four resolution levels. Therefore, three resolution levels were used in this work.

After wavelet transforming the images, an adaptive Wiener filter algorithm was applied to each approximation image obtained from the wavelet decomposition. The adaptive Wiener filter adaptively implements a pixel-by-pixel approach based on statistics estimated from local neighborhoods of each data point. The local filter is a space-variant lowpass filter whose Fourier transform is given by [17]:

$$H(u, v) = \frac{S_f(u, v)}{S_f(u, v) + S_\eta(u, v)} \quad (10)$$

where $S_f(u, v)$ and $S_\eta(u, v)$ are the power spectrum of the noise and the non-degraded image, respectively. Within the local region, the non-degraded image is assumed stationary, with mean m_f and variance σ_f^2 .

The adaptive algorithm then estimates the local mean and variance, defining an $N \times M$ neighborhood Δ around each pixel in the non-degraded image, referred to as $F(n_1, n_2)$, given by:

$$m_f = \frac{1}{NM} \sum_{n_1, n_2 \in \Delta} F(n_1, n_2) \quad (11)$$

$$\sigma_f^2 = \frac{1}{NM} \sum_{n_1, n_2 \in \Delta} F^2(n_1, n_2) - m_f^2 \quad (12)$$

The restored image \hat{F} is obtained from the restored local regions given by:

$$\hat{F}(n_1, n_2) = m_f + \frac{\sigma_f^2}{\sigma_f^2 + \sigma_\eta^2} (F(n_1, n_2) - m_f) \quad (13)$$

The noise variance is estimated from the average of all σ_f^2 . In this work, it was used a typical neighborhood Δ of size 3×3 . After the application of the Wiener filter to the approximation wavelet sub-image, the inverse transform was taken to return to the spatial domain.

2.3. Segmentation using wavelet analysis and genetic algorithm

After artifact removal and enhancement of mammograms, the segmentation algorithm developed by Hammouche et al. [21] was applied to the images to delineate the mass boundaries, followed by a post-processing algorithm. Hammouche's computational algorithm combines wavelet theory and genetic algorithm (GA) in order to determine the number

of thresholds for each mammographic image as well as the appropriate threshold levels, as described below.

Hammouche's algorithm description. At a first stage, a gray level histogram was computed to obtain a graphic representation of the gray level distribution for each image. To accelerate GA convergence, the histogram size must be reduced using a dyadic wavelet transform. The histogram is decomposed into approximate and detail signals. The approximate signal results in a reduced dimension version of the histogram, but still contains the characteristics of the original image histogram.

Let $h_g[i]$ be the original image histogram, with $i = 0, \dots, L - 1$, and L the gray levels of the considered image. Hence, for a wavelet resolution level j , the length of the reduced histogram $h_g^j[i]$ (approximate wavelet coefficients), denoted L_j , is given by $L_j = L/2^j$.

After histogram reduction, a GA was applied to determine the number of thresholds and its respective value. The GA purpose is to classify the mammographic image into k classes (C_1, C_2, \dots, C_k) with a set of threshold levels $T = \{t_0, t_1, \dots, t_k\}$, where, for convenience, it is assumed that $t_0 = 0$ and $t_k = L - 1$.

In the proposed GA, a chromosome is encoded as a binary string A of size L_j , such that $A = a_0, a_1, \dots, a_{L_j-1}$, where each character a_i corresponds to a 0 (zero) or 1 (one). If $a_i = 0$, the point $(i, h_g^j[i])$ indicates a valley, else it is a peak of the histogram. The position i for which $a_i = 0$ indicates a threshold value. As an example, let $L_j = 16$ and consider the string $A = 1101011101111111$. Then, the number of thresholds is 3 and the threshold values are $t_1 = 2$, $t_2 = 5$ and $t_3 = 9$. The initial population of chromosomes is randomly generated with a fixed size of P strings (A_1, A_2, \dots, A_P), and each string has L_j randomly generated bits. Due to its random nature, the chromosomes may contain a sequence of consecutive zeros, which is an undesirable behavior. To overcome such a situation, the algorithm keeps the first gene equal to zero and a mutation process changes the remaining zero-bits.

Let k be the classification number and $\text{Dis}[k]$ a discrepancy measure between the original and the thresholded images. The GA fitness function, used to classify the gray-levels as a number k , was computed following Yen et al. [22], and is given by:

$$\text{Fit}[k] = \rho \sqrt{\text{Dis}[k]} + (\log_2(k))^2 \quad (14)$$

where ρ is a positive weighting constant. The GA determines the optimal classification number k^* such that:

$$\text{Fit}[k^*] = \min_{k \in L_j^+} \text{Fit}[k] \quad (15)$$

where $L_j^+ = \{1, 2, \dots, L_j\}$. The discrepancy term is defined as:

$$\text{Dis}[k] = \sigma_T^2 - \sigma_B^2[k] \quad (16)$$

with σ_T^2 and σ_B^2 representing the between-class and the total class variances, respectively, given by:

$$\sigma_B^2 = \sum_{n=1}^k P_n(m_n - m)^2 \quad (17)$$

$$\sigma_T^2 = \sum_{n=0}^{L_j-1} (n - m)^2 p_n \quad (18)$$

where

$$P_i = \sum_{n=t_{i-1}}^{t_i-1} p_n, \quad m_i = \frac{\sigma_i}{P_i}, \quad \sigma_i = \sum_{n=t_{i-1}}^{t_i-1} n p_n,$$

$$m = \sum_{n=0}^{L_j-1} n p_n, \quad p_n = \frac{h_g^j[n]}{N} \quad (19)$$

with N the number of pixels of the mammographic image. In this step, the best string is marked as the best solution and copied to its neighboring values, i.e., t_1 is copied to $t_1 - 1$ and $t_1 + 1$. Then, the best string fitness value can be tested for a possible improvement observing those neighborhoods.

Following, the GA tournament selection process was applied for choosing the fittest individuals. For that, two strings A' and A'' of the current population were randomly selected and the string with the best fitness value was chosen to belong to the mating pool. This procedure was repeated until a mating pool is filled with the same size of the population.

A single crossover operation was performed on two randomly selected strings A' and A'' . A random integer number $q \in [0, L_j - 1]$ was generated and two offsprings were created by swapping all characters of A' and A'' after position q . Recombination was performed based on the value of the crossover probability P_c . A random number within $[0, 1]$ was associated to each pair of strings: if it was less than P_c , then crossover was performed, otherwise no crossover was employed.

Mutation, associated with a low probability P_m , was performed based on another random number generated within $[0, 1]$. If this value was less than P_m , then a character of the recombined string was randomly chosen and its value altered. To overcome a possible generation of successive zero-bits with mutation, the same approach of keeping only the first zero and changing the remaining was performed.

Since the threshold values determined by GA were obtained from a reduced histogram, these values must be expanded to their original spaces. For that, each threshold t_i is multiplied by a factor 2^j .

After the expansion, a refinement procedure was applied to obtain stable and more accurate threshold levels. In this procedure, the mean gray level $m_i[r]$ of the class C_i , $i = 1, 2, \dots, k - 1$, were computed, where r stands for the time of iteration. Then, the value of $t_i[r]$ were updated according to:

$$t_i[r + 1] = \frac{m_i[r] + m_{i+1}[r]}{2} \quad (20)$$

These steps were repeated until the iteration converges, i.e., $t_i[r + 1] = t_i[r]$ for $i = 2, 3, \dots, k - 1$.

After determining the threshold numbers and its values, the segmentation was finalized applying the expression:

$$B(x, y) = i \quad \text{if} \quad t_{i-1} \leq f(x, y) \leq t_i, \quad i = 1, 2, \dots, k. \quad (21)$$

where $f(x, y)$ is the original image and $B(x, y)$ is the segmented image.

The automatic segmentation algorithm was implemented using $P_c = 0.9$ and $P_m = 0.001$. The population size P depends on the chromosome size and the resolution level j of the wavelet transform. In this article, it is used $P = 150/2^j$ and GA is executed for 100 generations. As proposed by Hammouche et al. [21], the weighting constant ρ must depend on the resolution level and it was used the value $\rho = 0.5 \times 2^j$. The wavelet transform was performed with the Daubechies wavelet ‘db2’. It is important to distinguish the wavelet employed on the filtering algorithm to the one applied on the segmentation step, since they may use different wavelet functions, as it was indeed done in this article.

Post-processing algorithm. To reduce the number of possible false positives, a post-processing algorithm was employed in this step. This algorithm was developed in a semi-automatic way. The procedure was divided in two stages: the first compares the detected region shape with ones previously defined (automatic done by a software computer), and the second verifies the area of the region taking into account informations extracted from both mammographic views (CC and MLO). A specialist performs this second task manually.

In the first stage, the possibly abnormal regions identified by the procedure were separated (cropped) from the thresholded image, and area, center and perimeter measures were computed for each of those regions. After some observations of the areas computed for known regions, it was noted that abnormal areas ranged from 1000 to 40,000 squared pixels (pixel \times pixel). Based on these empirical observations obtained through previous experiments, it was developed an algorithm that analyzed, for each selected region, those with structural values above the established threshold areas and discarded them from being an abnormal regions. This procedure was applied to images from views CC and MLO, separately.

In the next step, the area of the remaining structures marked on the CC view was manually compared to that on the MLO view by a specialist. Only regions having 95% to 100% of area size agreement were preserved and marked as abnormal structures.

2.4. Performance evaluation

Performance evaluation was carried out in two ways, namely evaluation of the contrast enhancement algorithm and evaluation of the multimodal segmentation algorithm.

Enhancement using wavelet processing. To quantify the contrast enhancement filtering performance, regions of interest (ROIs) on the mammographic images were selected and the methods proposed by Singh and Bovis [23] and Pereira et al. [24] were used. The evaluation was performed comparing different wavelet functions. The snake active contour model was employed to separate the object (mass) area and the background area of the ROI.

Singh and Bovis' method comprises four different metrics, namely distribution separation measure (DSM), target-to-background contrast enhancement measurement based on standard deviation (TBC_s), target-to-background contrast enhancement measurement based on entropy (TBC_e) and combined enhancement measure (D). DSM quantifies the

overlap between the masses boundary and the background, before and after segmentation, and is given by:

$$DSM = (|M_2 - \mu_{bg}^P| + |M_2 - \mu_{ob}^P|) - (|M_1 - \mu_{bg}^O| + |M_1 - \mu_{ob}^O|) \quad (22)$$

where

$$M_1 = \frac{\mu_{bg}^O \sigma_{ob}^O + \mu_{ob}^O \sigma_{bg}^O}{\sigma_{ob}^O \sigma_{bg}^O + \varepsilon} \quad (23)$$

$$M_2 = \frac{\mu_{bg}^P \sigma_{ob}^P + \mu_{ob}^P \sigma_{bg}^P}{\sigma_{ob}^P \sigma_{bg}^P + \varepsilon} \quad (24)$$

and $\mu_{bg}^O, \sigma_{bg}^O, \mu_{ob}^O, \sigma_{ob}^O$ are the mean and standard deviation of the background and mass areas, respectively, of the original image. Similarly, $\mu_{bg}^P, \sigma_{bg}^P, \mu_{ob}^P, \sigma_{ob}^P$ are the mean and standard deviation of the background and mass areas, respectively, of the image after enhancement. The term ε is a very small constant used to prevent division by zero. The greater DSM, the better the enhancement.

The metrics TBC_s and TBC_e are used to measure the homogeneity of the mass, comparing the difference between background and mass mean gray-level, related to the image standard deviation and the entropy, respectively. These metrics are defined as:

$$TBC_s = \frac{(\mu_{ob}^P / \mu_{bg}^P) - (\mu_{ob}^O / \mu_{bg}^O)}{\sigma_{ob}^P / \sigma_{ob}^O} \quad (25)$$

$$TBC_e = \frac{(\mu_{ob}^P / \mu_{bg}^P) - (\mu_{ob}^O / \mu_{bg}^O)}{Ent_{ob}^P / Ent_{ob}^O} \quad (26)$$

where Ent_{ob}^O, Ent_{ob}^P are the entropy of the mass in the original and enhanced images, respectively. These metrics must have values greater than zero. Greater values indicate better results.

The combined enhanced measure D is an Euclidean distance between the scaled representation of the three metrics above in a 3D space and the point (1,1,1). This is given by:

$$D = \sqrt{(1 - DSM)^2 + (1 - TBC_s)^2 + (1 - TBC_e)^2} \quad (27)$$

The smallest Euclidean distance represents the best enhancement technique.

The metric proposed by Pereira et al. evaluates the enhancement algorithm in relation to the differences between the mean gray-levels of the background and the mass, and is defined as:

$$CNR = \frac{(\mu_{ob}^P - \mu_{bg}^P)}{\sqrt{(\sigma_{ob}^P)^2 + (\sigma_{bg}^P)^2 / 2}} \quad (28)$$

Segmentation using wavelet analysis and genetic algorithm. To evaluate the performance of the proposed segmentation algorithm, the lesion nodule area was computed and compared to the areas marked by an expert radiologist. Assuming that A is the computer-segmented contour and B is the manually

segmented contour, the area overlap measure (AOM) is given by:

$$AOM = \frac{\text{Area}(A \cap B)}{\text{Area}(A \cup B)} \quad (29)$$

This general area metric, defined as a percentage, has been used by several authors to evaluate the performance of segmentation algorithms [25–27]. The higher the AOM is, the better the segmentation will be, where an ideal value would be equal to 1.

2.5. Data set

The database used in this work encompasses mammographic screen/film digitalized images taken from the Digital Database for Screening Mammography (DDSM) [12]. The DDSM project is a joint effort of researchers from the Massachusetts General Hospital (D. Kopans, R. Moore), the University of South Florida (K. Bowyer), and the Sandia National Laboratories – EUA (P. Kegelmeyer). The DDSM database has been widely used as a benchmark for numerous articles on the mammographic area, for being free of charge and having a vast and diverse quantity of cases. It is constituted of mammographic images and its corresponding technical and clinical informations, including exam dates, age of patients, digitalization equipment (as well as resolution, number of rows, pixels per row and bits per pixel of the acquired images), lesion types and existent pathologies.

For the evaluation of the enhancement method and segmentation algorithm, a data set was used comprising 640 mammographic images from 160 patients (being 80 with benign and 80 with malignant lesions) which were randomly selected from DDSM dataset. These lesions have different sizes, densities, and margins types. For each case, we used four mammograms, taken from the left and the right breasts, obtained in CC and MLO views. We selected images digitized with a Lumisys laser film scanner at 50 mm and a Howtek scanner at 43.5 mm pixel size. Each image has a resolution of $M = 2^{12} = 4096$ gray level tones. The information provided by the radiologists and their opinions are the main sources to validate the algorithm. Thus, the results achieved with the algorithm proposed in the present article have been compared to those provided by the DDSM.

3. Results and discussion

This section presents the results achieved by the proposed computational algorithms for the enhancement, detection and segmentation steps applied for mammographic images. The proposed procedure was tested on a PC with an i7 microprocessor with 6 cores, 8 GB of RAM and a hard disk of 250 GB. The time spent for each pair of CC/MLO image was 11.05 s.

3.1. Segmentation using wavelet analysis and genetic algorithm

To show examples of the automatic segmentation algorithm outcomes, we selected two cases, A_1347 and C_0031, from the 160 cases analyzed. These nomenclatures were taken from the DDSM project website, which uses a code to each of the

Table 1 – Results obtained with enhancement filter based on Haar wavelet transform.

| Image | DSM | TBC _s | TBC _e | D | CNR |
|------------|--------|------------------|------------------|--------|---------|
| A_1347_CC | 1.1240 | 0.0013 | 0.0006 | 1.6444 | 13.6372 |
| A_1347_MLO | 1.2351 | 0.0022 | 0.0017 | 1.4892 | 18.3579 |
| C_0031_CC | 1.0774 | 0.0037 | 0.0039 | 1.5875 | 15.1276 |
| C_0031_MLO | 1.2918 | 0.0049 | 0.0047 | 1.4374 | 15.9844 |

Table 2 – Results obtained with enhancement filter based on Daubechies wavelet transform.

| Image | DSM | TBC _s | TBC _e | D | CNR |
|------------|--------|------------------|------------------|--------|---------|
| A_1347_CC | 1.1291 | 0.0015 | 0.0004 | 1.5456 | 10.4260 |
| A_1347_MLO | 1.2484 | 0.0025 | 0.0012 | 1.4811 | 25.5305 |
| C_0031_CC | 1.1205 | 0.0037 | 0.0027 | 1.4992 | 12.8887 |
| C_0031_MLO | 1.1554 | 0.0038 | 0.0045 | 1.4801 | 9.4567 |

available mammography cases differentiating them by the scanner used to digitalize it (capitalized letter) and the patient code (number). The reader should refer to [12] for further details. Fig. 4(a) and (b) shows the left breast for both views of case A_1347, with a malignant lesion, and Fig. 4(c) and (d) shows the two left breast visions of case C_0031, with a benign lesion.

Fig. 5(a) and (b) shows results obtained by the segmentation algorithm for CC and MLO views of case A_1347, respectively. With GA application, the threshold values computed were 1, 10, 21, 35, 54, 78, 104, 130, 155, 175, 194, and 226. In Fig. 5(c) and (d), we show the images produced by the segmentation algorithm for CC and MLO views of case C_0031, respectively. For this case, GA application resulted in threshold values 1, 31, 58, 68, 82, 99, 118, 137, 151, 163, 181, and 213. It can be observed that several regions were identified as abnormalities, even when it was not actually present, what characterizes false positives. That was the case for the pectoral muscle, for example. This behavior was due to the use of bright level intensities to define regions, which in some cases are not uniform.

The results after the post-processing proposed method are shown in Fig. 6(a) and (b) for the CC and MLO views of case A_1347, respectively, and in Fig. 6(c) and (d) for the CC and MLO views of case C_0031, respectively. It can be observed from the examples that, after the post-processing step, the number of false positive regions was decreased or even fully eliminated.

Other examples of correctly segmentation masses from the database are presented in Fig. 7, where the algorithm successfully provides precise boundary of masses ranging from subtle to obvious.

3.2. Enhancement based on wavelet multiresolution processing evaluation

The performance of the contrast enhancement algorithm was evaluated for three wavelet families, namely Haar, Daubechies and Coiflet, by means of the metrics DSM, TBC_s, TBC_e, D and CNR defined in the previous section. Tables 1–3 show the results obtained by the enhancement filters applied to both CC and MLO views for the cases A_1347 and C_0031 taken from the DDSM data set.

It can be inferred from these tables that Coiflet-based wavelet transform provided, in general, better results,

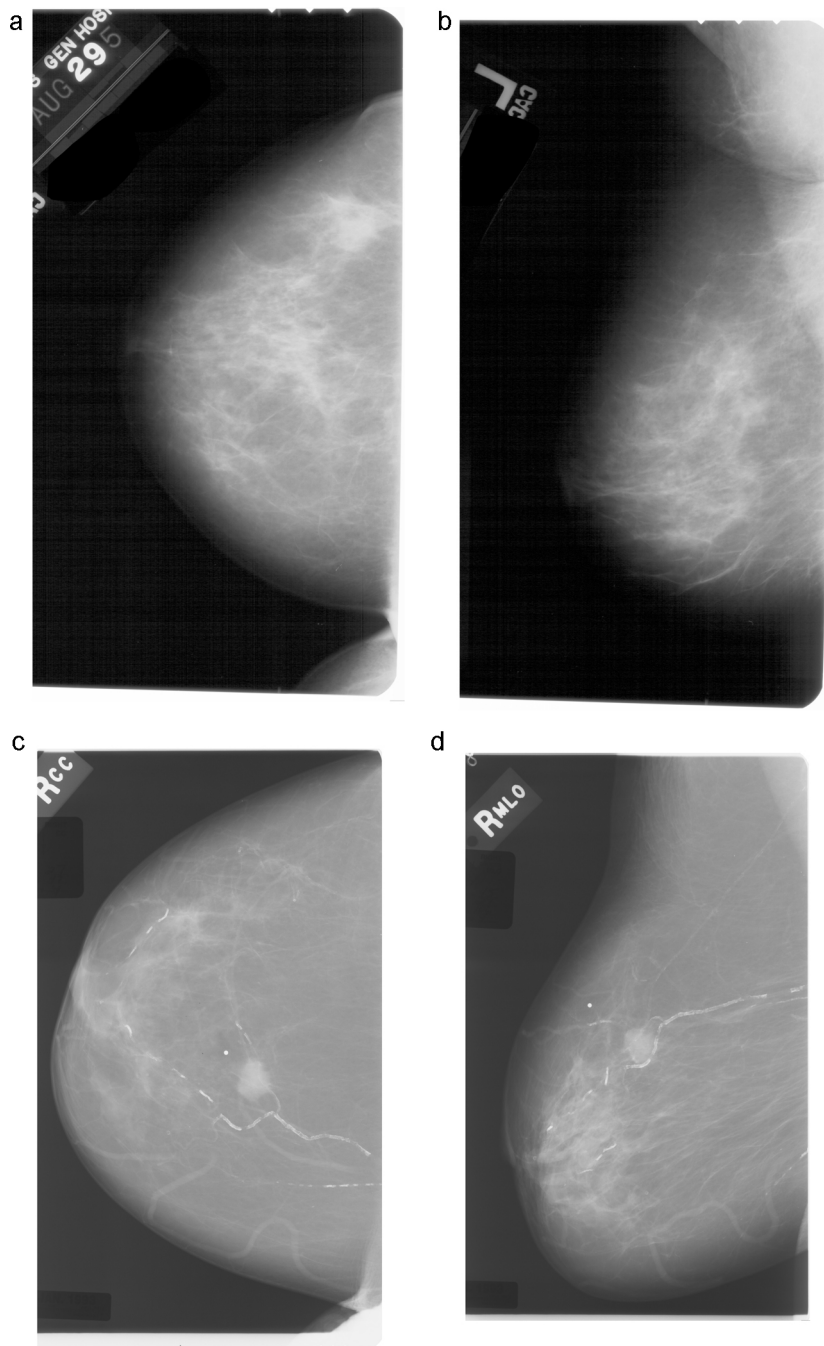


Fig. 4 – Original images: (a) CC view of case A_1347; (b) MLO view of case A_1347; (c) CC view of case C_0031; (d) MLO view of case C_0031.

| Table 3 – Results obtained with enhancement filter based on Coiflet wavelet transform. | | | | | |
|---|--------|------------------|------------------|--------|---------|
| Image | DSM | TBC _s | TBC _e | D | CNR |
| A_1347_CC | 1.5832 | 0.0018 | 0.0006 | 1.5281 | 27.9584 |
| A_1347_MLO | 1.4365 | 0.0026 | 0.0014 | 1.4773 | 28.1691 |
| C_0031_CC | 1.3293 | 0.0049 | 0.0041 | 1.4458 | 17.3036 |
| C_0031_MLO | 1.1624 | 0.0040 | 0.0033 | 1.4830 | 11.2501 |

considering all metrics defined above. Indeed, that was the case, in average, for all metrics applied to the 160 selected cases. We have computed those metrics and their values were averaged for each wavelet family.

For the DSM metric, the mean value for all selected cases was 1.52 for the Coiflet wavelet, 1.23 for Haar wavelet and 1.26 for Daubechies wavelet, showing that Coiflet was 19% better than the worst, Haar wavelet. For the TBC_s metric, this behavior remained the same, once its mean value for the Coiflet wavelet was 0.0043, against 0.003 for Haar and 0.034 for Daubechies wavelets. The same superiority was obtained

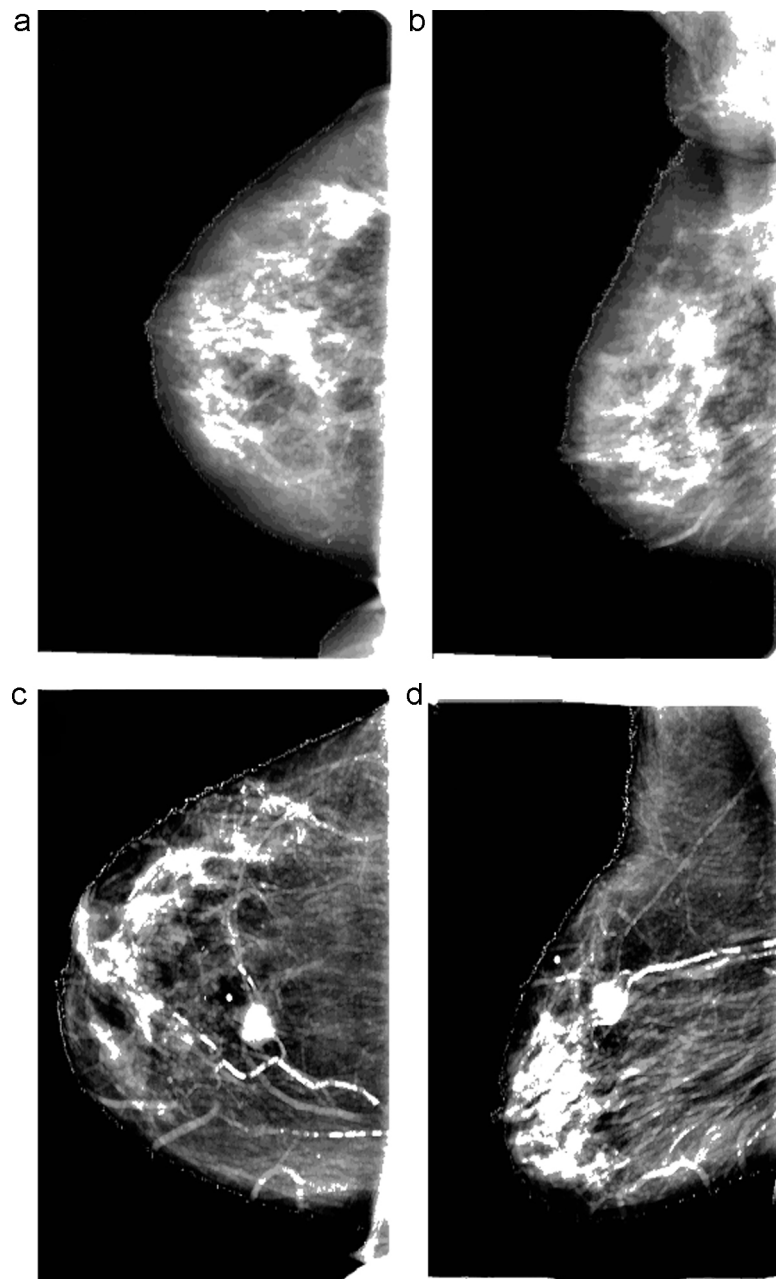


Fig. 5 – Segmented images: (a) CC view of case A.1347; (b) MLO view of case A.1347; (c) CC view of case C.0031; (d) MLO view of case C.0031.

for the TBC_e metric, were Coiflet wavelet presented a mean value of 0.0053, while Haar and Daubechies wavelets presented 0.0041 and 0.0044, respectively. When combining these metrics into the Euclidean distance D , Coiflet was still superior, presenting a mean value of 1.35, against 1.20 and 1.13 for Haar and Daubechies wavelets, respectively. The same occurred for the CNR metric, where it was obtained a mean value of 23.06 for the Coiflet wavelet, 17.52 for the Haar wavelet and 16.83 for the Daubechies wavelet.

Therefore, considering all metrics of Singh & Bovis and Pereira et al., the filter based on Coiflet wavelet was more efficient for the enhancement step of the CADe proposed system. A reasonable justification on why this may happen seems to be

that, besides having more symmetry and vanishing moments than the others wavelets, Coiflet basis satisfy the mini-max condition, what means that the maximum error for estimation is minimized.

3.3. Segmentation evaluation

The average AOM achieved by our segmentation algorithms is approximately $0.79 \pm 8\%$. Considering the AOM percentage, for all selected cases, this is equivalent to 79%, on average, of overlap between the ground truth regions and the automatically segmented regions. The AOM value indicates the percentage difference between the areas of the automatic and

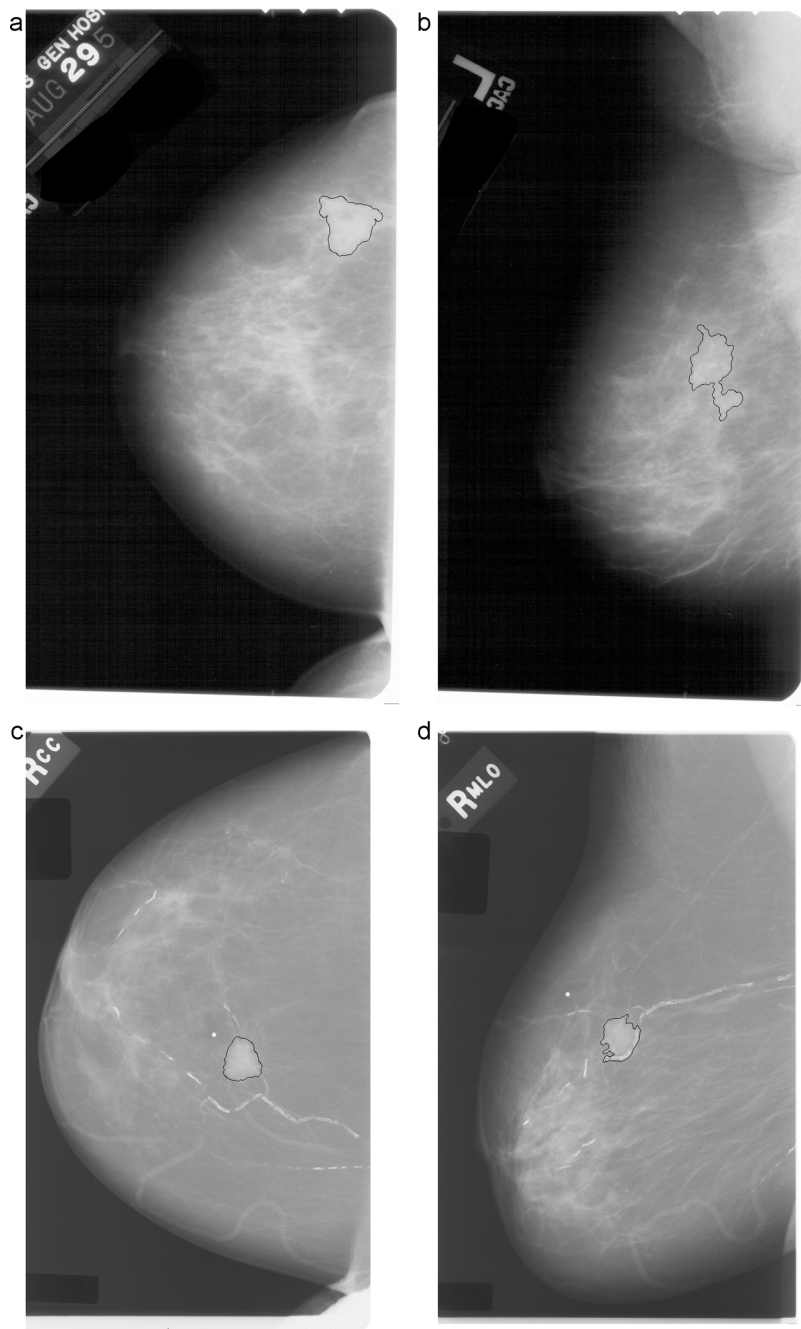


Fig. 6 – Images after post-processing step: (a) CC views of case A_1347; (b) MLO views of case A_1347; (c) CC view of case C_0031; (d) MLO view of case C_0031.

the manual selection. As described by Timp and Karssemeijer [28], the segmentation methods rarely achieve an AOM value 90% or higher. One reason for this is that the accuracy of the manually segmented regions is limited. Often the manual segmentations are somewhat large to make sure the whole tumor is inside the annotation.

Fig. 8(a)–(d) shows, respectively, the ROIs marked by the chain code and the proposed method for CC and MLO views of case A_1347. The ROIs identified by the chain code and the proposed method for CC and MLO views of case C_0031 are presented, respectively, in Fig. 8(e)–(h). It can be verified from

Table 4 – Average number of true positive and false positive regions after post-processing step

| | True positive (%) | False positive |
|---------------------------------|-------------------|----------------|
| First stage of post-processing | 95 | 2.80 |
| Second stage of post-processing | 95 | 1.37 |

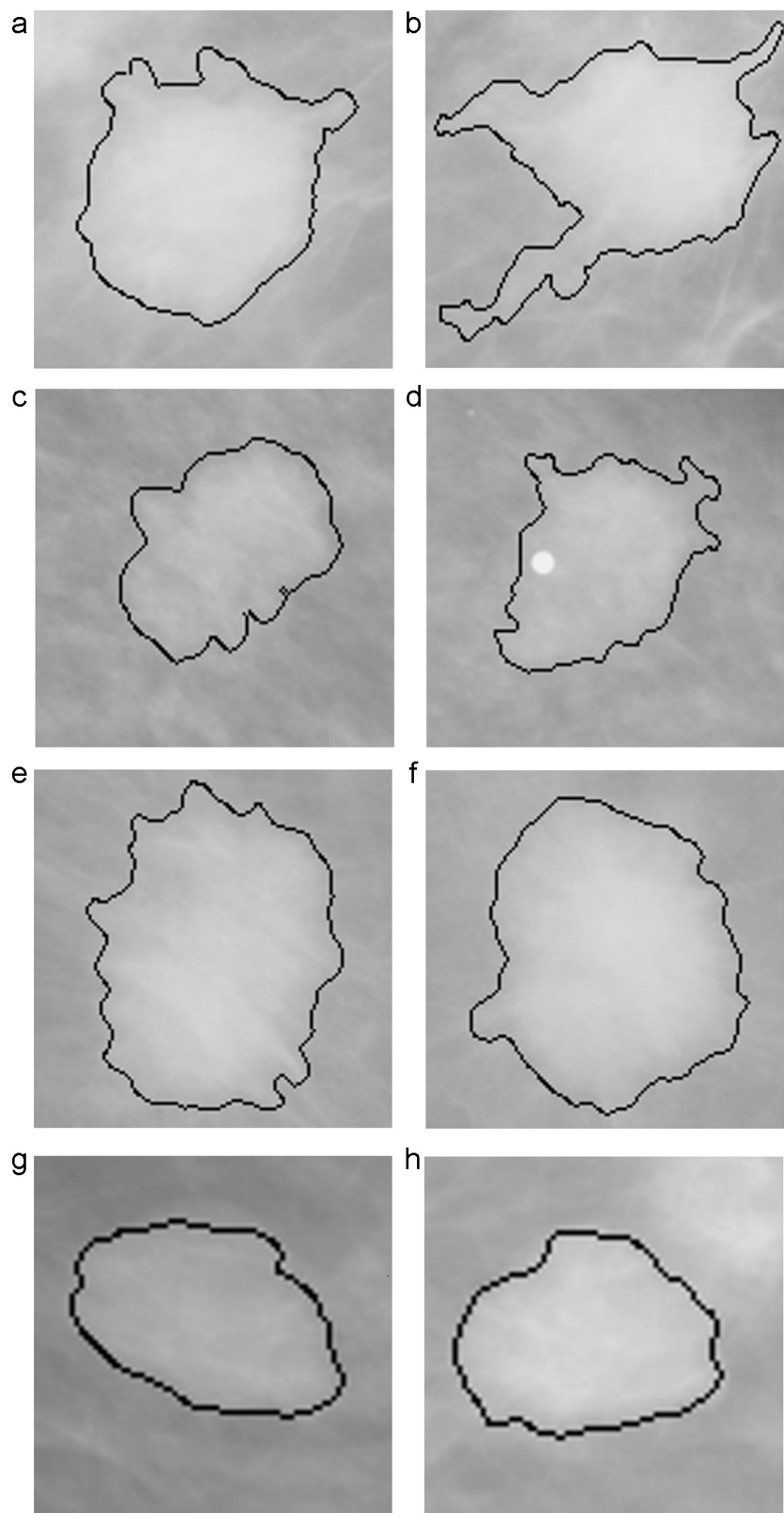


Fig. 7 – Examples of segmentation masses in others cases of DDSM database: (a) CC view of C.0009; (b) MLO view of C.0009; (c) CC view of C.0023; (d) MLO view of C.0023; (e) CC view of C.0037; (f) MLO view of C.0037; (g) CC view of C.0332; (h) MLO view of C.0332.

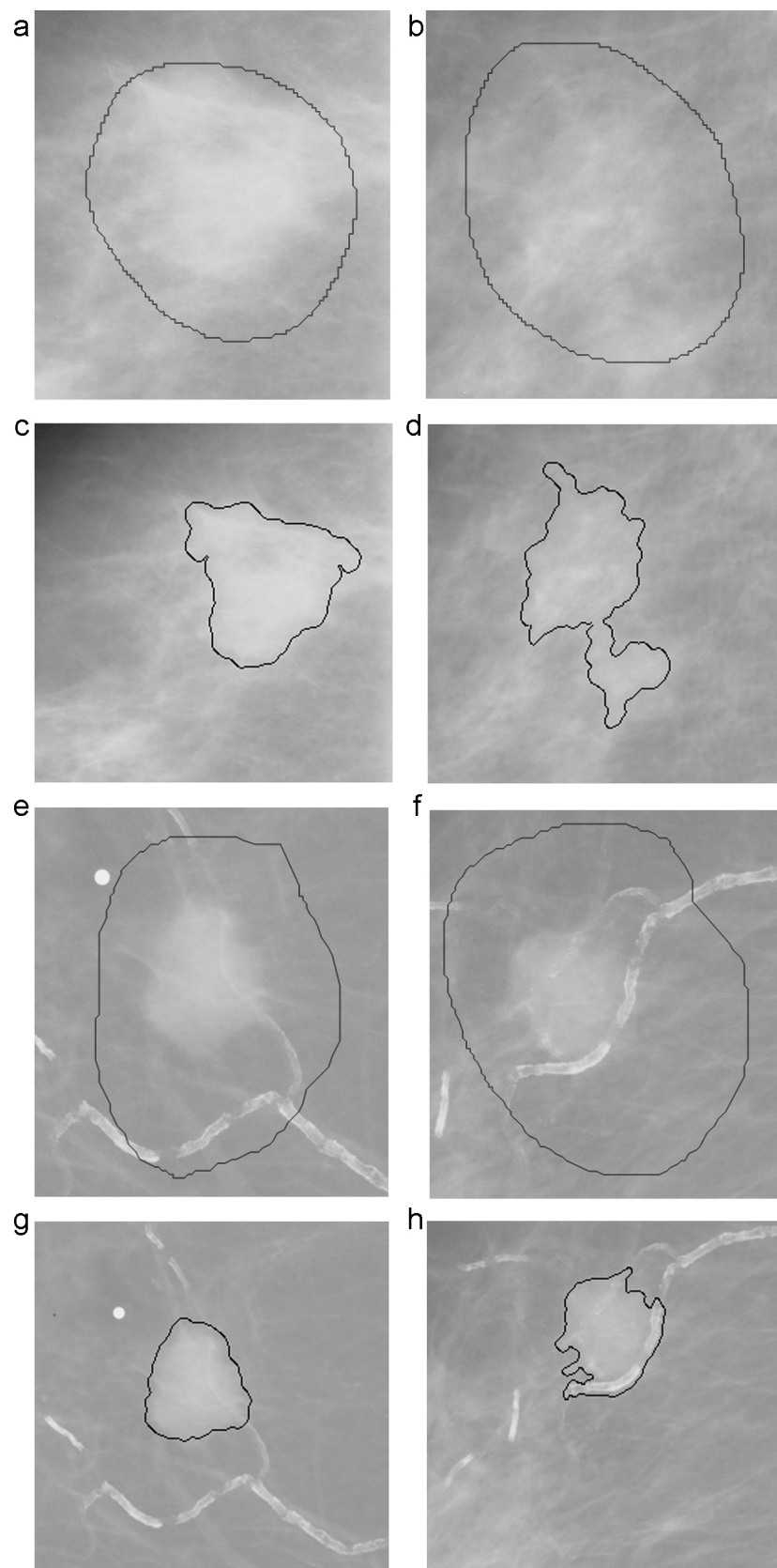


Fig. 8 – Regions of interest: (a) and (b) CC and MLO visions of case A_1347 marked by the chain code; (c) and (d) CC and MLO visions of case A_1347 marked by the proposed method; (e) and(f) CC and MLO visions of case C_0031 marked by the chain code; (g) and (h) CC and MLO visions of case C_0031 marked by the proposed method.

Table 5 – Performance comparison.

| Algorithm | Sensitivity (%) | FP/image | Database | Number of images | Use of two-views |
|--------------------------|-----------------|----------|--|------------------|------------------|
| Paquerault et al. [10] | 73 | 1 | Breast Image Division – University of Michigan | 169 | Yes |
| Van Engeland et al. [11] | 83 | 1 | Not informed | 948 | Yes |
| Wei et al. [29] | 83.7 | 1 | Department of Radiology – University of Michigan | 23,332 | Yes |
| Hu et al. [32] | 91.3 | 0.71 | MIAS | 172 | No |
| This work | 95 | 1.37 | DDSM | 640 | Yes |

Fig. 8(a), (c), (e), and (g) that the chain code identifies abnormalities in an unsatisfied way, since for several cases part of the background (tissue with no masses) is selected in this process. This behavior was also perceived in the work of Menecattini et al. [20]. With the proposed method, shown in **Fig. 8(b), (d), (f), and (h)**, the mass border is more precisely delineated compared to the chain code. This allows for the specialist to classify in a more accurate manner if the abnormality is malignant or benign.

3.4. Detection evaluation

Table 4 shows the average number of TP and FP per image for the set of selected cases. In that table, there is a line corresponding to the first stage of the post-processing algorithm and a line corresponding to the second stage. A ROI is identified as a true positive case if there is a mass and the algorithm selects it. The true positive rate is also known as sensitivity. A false positive occurs when the algorithm selects a mass when there is none at that location. Hence, as stated by **Table 4**, the proposed method acquired a sensitivity of 95%, for both the first and second stages. The number of false positive ROIs per image was 2.8 for the first stage and 1.37 for the second stage. These results reveal that the proposed method outcomes are better than some previous works found in literature, as stated in the next few paragraphs and summarized in **Table 5**.

The algorithm proposed by Paquerault et al. [10] presented a FP rate of 1 FP/image with a sensitivity of 73%. The authors made use of a geometrical model to predict object location in one view, based on the other one. After the mass-pairing step, a linear discriminant analysis was performed to classify the object. The dataset used, composed of 169 mammograms, was selected from patient files in the Breast Image Division at the University of Michigan.

Van Engeland et al. [11] obtained a FP rate of 1 FP/image with a sensitivity of 83%. On their work, using correspondence between regions, the authors built a cascaded multiple-classifier system and two-view analysis to obtain a CAD system. The dataset was composed of 948 images mammograms and it was not informed where these images were obtained.

The method proposed by Wei et al. [29] reached 1 FP/image at a sensitivity of 83.7%. The authors used image registration to identify potential pairs on both CC and MLO views and similarity measures to differentiate True-Positive/True-Positive pairs from other pairs. After that, a linear discriminant analysis was performed for classification. A total of 2332 mammograms

were used, collected from patient files of the Department of Radiology at the University of Michigan.

The method proposed by Hu et al. [32] reached a sensitivity of 91.3% at 0.71 FP per image. The algorithm utilized a combination of global adaptive thresholding and local adaptive thresholding for mass segmentation on a multiresolution representation of the images. The MIAS dataset was used, comprised of 172 mammograms.

4. Conclusion

In this article, we have developed a computational method to detect and segment regions in mammographic images using genetic algorithm and multiresolution techniques. A pre-processing method based on wavelet transform and Wiener filtering was applied for image denoising and enhancement. Genetic algorithm was then employed for segmentation of suspicious regions, followed by a post-processing step that took into account information contained in CC and MLO views. The segmentation algorithm was applied to 640 mammographic images from 160 cases and resulted in an AOM of 0.79. The experiments demonstrate that the proposed method has a strong potential to be used as the basis for mammogram mass segmentation in CC and MLO views. A FP rate of 1.35 FP/image was acquired for a sensitivity of 95%. This detection rate of benign and malignant lesions indicates that this method may be applied as a tool to assist radiologist in breast cancer diagnosis. However, the post-processing procedure implemented in this work must be improved, by turning it into a completely automatic algorithm as well using some algorithm for correspondence of regions for both CC and MLO views.

Although the proposed scheme presented a relatively high accuracy results, it is the authors' intention to investigate the use of other types of multiresolution transforms. One such a transform that has been under investigation on the literature is the complex-wavelet transform (CWT), which presents some advantages as shift insensibility, directionality and phase information [30]. The curvelet and shearlet transforms are another examples of possible future investigation as a way to improve the efficiency of the proposed algorithm, for having directional information as well [30,31]. Another future study direction is the investigation of false positive reduction algorithms evaluated by means of FROC curves. These algorithms may improve even more the performance of the proposed system.

Acknowledgment

The authors would like to thank the financial support of FAPESP (Fundação de Amparo à Pesquisa do Estado de São Paulo).

REFERENCES

- [1] World Health Organization, Cancer, Fact Sheet No. 297, available at: <http://www.who.int/mediacentre/factsheets/fs297/en> (accessed September 2011).
- [2] Brasil, Ministério da Saúde, Instituto Nacional do Câncer (INCA), Estimativa 2010, Incidência de câncer no Brasil, http://www.inca.gov.br/estimativa/2010/estimativa2010_1201.pdf (accessed September 2011).
- [3] J. Tang, R.M. Rangayyan, J. Xu, N. El, Y. Yang, Computer-aided detection and diagnosis of breast cancer with mammography: recent advances, *IEEE Transactions on Information Technology in Biomedicine* 13 (2009) 236–251.
- [4] M. Elter, A. Horsch, CADx of mammographic masses and clustered microcalcifications: a review, *Medical Physics* 36 (2009) 2052–2068.
- [5] M.L. Giger, H.P. Chan, J. Boone, Anniversary paper: history and status of CAD and quantitative image analysis: the role of medical physics and AAPM, *Medical Physics* 35 (2008) 5799–5820.
- [6] A. Olivera, J. Freixeneta, J. Martí, E. Pérez, B. Ponte, E.R.E. Dentonc, R. Zwiggelaard, A review of automatic mass detection and segmentation in mammographic images, *Medical Image Analysis* 14 (2010) 87–110.
- [7] B.W. Hong, B.S. Sohn, Segmentation of regions of interest in mammograms in a topographic approach, *IEEE Transactions on Information Technology in Biomedicine* 14 (2010) 129–139.
- [8] S. Gupta, P.F. Chyn, M.K. Markey, Breast cancer CADx based on BI-RADS descriptors from two mammographic views, *Medical Physics* 33 (2006) 1810–1817.
- [9] B. Sahiner, H.P. Chan, L.M. Hadjiiski, M.A. Helvie, C. Paramagul, J. Ge, J. Wei, C. Zhou, Joint two-view information for computerized detection of microcalcifications on mammograms, *Medical Physics* 33 (2006) 2574–2585.
- [10] S. Paquerault, N. Petrick, H.P. Chan, S. Sahiner, M.A. Helvie, Improvement of computerized mass detection on mammograms: fusion of two-view information, *Medical Physics* 29 (2002) 238–247.
- [11] S.V. Engeland, N. Karssemeijer, Combining two mammographic projections in a computer aided mass detection method, *Medical Physics* 34 (2007) 898–905.
- [12] M. Heath, K. Bowyer, D. Kopans, R. Moore, W.P. Kegelmeyer, The Digital Database for Screening Mammography, in: Proceedings of the Fifth International Workshop on Digital Mammography, 2001, pp. 212–218.
- [13] N. Otsu, A threshold selection method from gray level histograms, *IEEE Transactions on Systems, Man, and Cybernetics* 40 (1992) 902–914.
- [14] H. Wang, J.-B. Li, L. Wu, H. Gao, Mammography visual enhancement in CAD-based breast cancer diagnosis, *Clinical Imaging* 37 (2013) 273–282.
- [15] N.-C. Tsai, H.-W. Chen, S.-L. Hsu, Computer-aided diagnosis for early-stage breast cancer by using wavelet transform, *Computerized Medical Imaging and Graphics* 35 (2013) 1–8.
- [16] R. Gonzalez, R. Woods, *Digital Image Processing*, 3rd ed., Pearson/Prentice Hall, New Jersey, USA, 2008.
- [17] J. Lim, *Two-dimensional Signal and Image Processing*, Prentice Hall, New Jersey, USA, 1990.
- [18] S. Mallat, Wavelets for a vision, *Proceedings of IEEE* 84 (1996) 604–614.
- [19] S. Mallat, *A Wavelet Tour of Signal Processing*, 2nd ed., Academic Press, California, USA, 1999.
- [20] A. Mencattini, M. Salmeri, R. Lojacono, M. Frigerio, F. Caselli, Mammographic images enhancement and denoising for breast cancer detection using dyadic wavelet processing, *IEEE Transactions on Instrumentation and Measurement* 57 (2008) 1422–1430.
- [21] K. Hammouche, M. Diaf, P. Siarry, A multilevel automatic thresholding method based on a genetic algorithm for a fast image segmentation, *Computer Vision and Image Understanding* 109 (2008) 163–175.
- [22] J.C. Yen, F.J. Chang, S. Chang, A new criterion for automatic multilevel thresholding, *IEEE Transactions on Image Processing* (1995) 370–378.
- [23] S. Singh, K. Bovis, An evaluation of contrast enhancement techniques for mammographic breast masses, *IEEE Transactions on Information Technology in Biomedicine* 9 (2005) 109–119.
- [24] C.S. Pereira, A.M. Mendonça, A. Camplilho, Evaluation of contrast enhancement filters for lung nodule detection, *LNCS* 4633 (2007) 878–888.
- [25] Y. Yuan, M.L. Giger, H. Li, K. Suzuki, C. Sennett, A dual-stage method for lesion segmentation on digital mammograms, *Medical Physics* 34 (2007) 4180–4193.
- [26] A.R. Domínguez, A.K. Nandi, Improved dynamic-programming-based algorithms for segmentation of masses in mammograms, *Medical Physics* 34 (2007) 4256–4269.
- [27] E. Song, L. Jiang, R. Jin, L. Zhang, Y. Yuan, Q. Li, Breast mass segmentation in mammography using plane fitting and dynamic programming, *Academic Radiology* 16 (2009) 826–835.
- [28] S. Timp, N. Karssemeijer, A new 2D segmentation method based on dynamic programming applied to computer aided detection in mammography, *Medical Physics* 31 (2004) 958–971.
- [29] J. Wei, H.P. Chan, B. Sahiner, C. Zhou, L.M. Hadjiiski, M.A. Roubidoux, M.A. Helvie, Computer-aided detection of breast masses on mammograms: dual system approach with two-view analysis, *Medical Physics* 36 (2009) 4451–4460.
- [30] V. Alarcon-Aquino, O. Starotensko, J.M. Ramirez-Cortez, et al., Detection of microcalcifications in digital mammograms using the dual-tree complex wavelet transform, *Engineering Intelligent Systems* 1 (2009) 49–63.
- [31] S. Zhou, J. Shi, J. Zhu, Y. Cai, R. Wang, Shearlet-based texture feature extraction for classification of breast tumor in ultrasound image, *Biomedical Signal Processing and Control* 8 (2013) 688–696.
- [32] K. Hu, X. Gao, F. Li, Detection of suspicious lesions by adaptive thresholding based on multiresolution analysis in mammograms, *IEEE Transactions on Instrumentation and Measurement* 60 (2011) 462–472.